Earth Syst. Dynam., 16, 2087–2100, 2025 https://doi.org/10.5194/esd-16-2087-2025 © Author(s) 2025. This work is distributed under the Creative Commons Attribution 4.0 License.





Conditions for instability in the climate—carbon cycle system

Joseph Clarke^{1,2}, Chris Huntingford³, Paul D. L. Ritchie^{1,2}, Rebecca Varney^{1,4}, Mark S. Williamson^{1,2}, and Peter Cox^{1,2}

Correspondence: Joseph Clarke (j.j.clarke@exeter.ac.uk)

Received: 30 July 2025 – Discussion started: 18 August 2025 Revised: 29 October 2025 – Accepted: 5 November 2025 – Published: 20 November 2025

Abstract. The climate and carbon cycle interact in multiple ways. An increase in carbon dioxide in the atmosphere warms the climate through the greenhouse effect, but also leads to uptake of CO₂ by the land and ocean sink, a negative feedback. However, the warming associated with a CO₂ increase is also expected to suppress carbon uptake, a positive feedback. This study addresses the question: "under what circumstances could the climate-carbon cycle system become unstable?" It uses both a reduced form model of the climate-carbon cycle system as well as the complex land model JULES, combined with linear stability theory, to show that: (i) the key destabilising loop involves the increase in soil respiration with temperature; (ii) the climate-carbon system can become unstable if either the climate sensitivity to CO₂ or the sensitivity of soil respiration to temperature is large, and (iii) the climate-carbon system is stabilized by land and ocean carbon sinks that increase with atmospheric CO₂, with CO₂-fertilization of plant photosynthesis playing a key role. For central estimates of key parameters, the critical equilibrium climate sensitivity (ECS) that would lead to instability at current atmospheric CO₂ lies between about 11 K (for large CO₂ fertilization) and 6 K (for no CO₂ fertilization). Given the apparent stability of the climate-carbon cycle, we can view these parameter combinations as implausible. The latter value is close to the highest ECS values amongst the latest Earth Systems Models. Contrary to a previous study that did not include an interactive ocean carbon cycle sink, we find that the stability of the climate-carbon system increases with atmospheric CO₂, such that the glacial CO₂ concentration of 190 ppmv would be unstable even for ECS greater than around 4.5 K in the absence of CO₂ fertilization of land photosynthesis.

1 Introduction

Earth's climate and carbon cycle are intimately coupled. Variations in global mean temperature throughout Earth's history have been linked to changes in atmospheric CO₂ concentrations (Zachos et al., 2001; Judd et al., 2024). The glacial-interglacial cycles that have occurred over the last 800 000 years are associated with ice-sheet dynamics and Milankovitch orbital forcing, but changes in CO₂ concentration have also played a role in significantly amplifying the

glacial to interglacial differences (Petit et al., 1999; Marcott et al., 2014).

Since the mid-nineteenth century atmospheric CO₂ concentrations have increased by 50% due to anthropogenic emissions from fossil fuel burning and deforestation, which has driven global warming through an enhanced greenhouse effect (Chen et al., 2021). The carbon cycle has played an important role here, absorbing about half of the anthro-

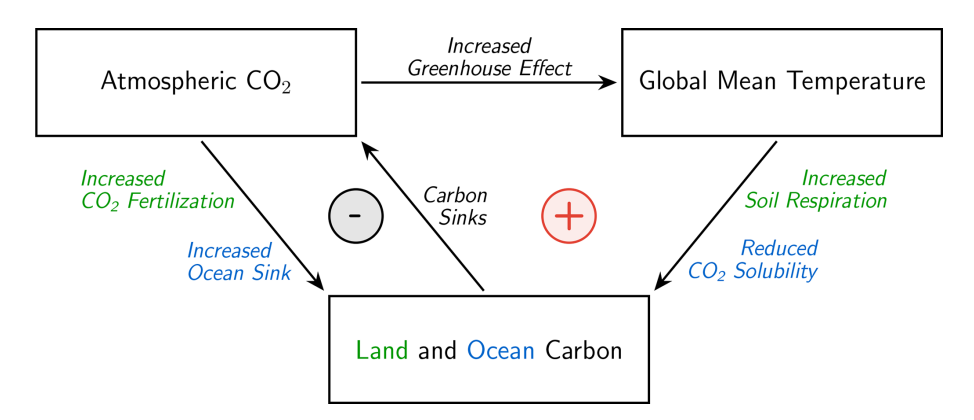


Figure 1. A schematic of the climate–carbon cycle interactions and feedbacks relevant to this study. This shows the negative (stabilising) increased CO₂ leading to increased carbon sink feedback loop, and the positive (destabilising) increased global temperatures leading to a reduced carbon sink feedback loop.

pogenic emissions of CO₂ through land and ocean carbon sinks (Canadell et al., 2021).

Contemporary land and ocean carbon sinks are the net effect of positive (amplifying) and negative (dampening) feedback loops (see Fig. 1). Increases in atmospheric CO₂ lead to an imbalance between the atmosphere and the surface ocean which results in additional CO₂ being dissolved in seawater and ultimately exported to depth by ocean circulations and marine biota (DeVries, 2022). In the absence of major nutrient limitations, the extra atmospheric CO₂ also increases the photosynthetic rates of land plants, which enables them to store more carbon and create the land carbon sink (Schimel et al., 2015). Both of these effects lead to an increased carbon sink due to increased CO₂. Therefore, they act to dampen an initial CO₂ perturbation (i.e. they are negative feedbacks).

The radiative forcing due to CO₂ leads to increases in global temperatures, which cause predominantly amplifying feedbacks (i.e. positive feedbacks). The positive feedbacks are particularly apparent on the land where the rate of heterotrophic respiration from the soil is known to increase significantly with warming (Davidson and Janssens, 2006; Jenkinson et al., 1991). Enhanced respiration on the land due to CO₂-induced warming is therefore projected to counteract CO₂-fertilization (Friedlingstein et al., 2006, 2014; Arora et al., 2020). In one early model, this increased temperatures leading to a reduced sink effect eventually overwhelmed CO₂ fertilisation of photosynthesis in the mid-21st century, converting the global land carbon sink into a source and significantly accelerating climate change (Cox et al., 2000).

This latter result amounted to a net positive feedback of the carbon cycle on anthropogenic climate change (feedback gain factor, g > 0), but it did not lead to an instability or "runaway" (which requires g > 1), in which small perturbations to atmospheric carbon grow rapidly. A subsequent analysis explored the conditions that could have led to a runaway climate—carbon cycle feedback (Cox et al., 2006), concluding that this would require at least one of the Equilibrium

Climate Sensitivity (ECS) or sensitivity of soil respiration to temperature to be unrealistically high (e.g. respiration increasing by a factor of 6 or more for every 10 K of warming), and that the climate–carbon cycle would become less stable with increases in the CO₂ concentration due to the saturation of CO₂ fertilization at high-CO₂.

In this study we reconsider the potential instability of the coupled climate–carbon system, for two main reasons. Firstly, we note that the upper range of ECS values has increased significantly in the CMIP6 generation of Earth System Models (ESMs), with some models now recording ECS values of up to 6 K (Zelinka et al., 2020). This increases the probability that some ESMs could suffer a climate–carbon cycle instability. Secondly, the Cox et al. (2006) study did not include the important stabilising effect of an interactive ocean carbon cycle, instead assuming that a fixed fraction of any atmospheric CO₂ perturbation would be taken up instantaneously by the ocean.

We use a more sophisticated representation of the ocean carbon cycle, alongside more complete representations of global warming and land carbon feedbacks, to answer the question: "under what circumstances could the climate–carbon cycle system become unstable?". To do this we perform a bifurcation analysis, which is a analysis of how the stability of a system changes as parameters change, of a conceptual model of the climate–carbon system and find our results are consistent with the output of the complex JULES global land-surface model (Clark et al., 2011; Best et al., 2011).

2 Conceptual model

To investigate the stability of the carbon-climate system, we construct a low dimensional model which represents important climate-carbon processes. We do this by combining existing models of components of the climate-carbon cycle system. This model can be analysed to determine critical pa-

rameter values that lead to a bifurcation and can be easily integrated numerically across a range of parameter values to determine its stability.

The model is composed of a climate component which models global temperature anomalies and a carbon cycle component which calculates the fluxes of carbon between the atmosphere, land and ocean. Very slow carbon cycle processes, such as the flux of carbon into and out of the solid Earth, and variations in astronomical forcing are neglected. As a result this model is not valid for longer than millennial timescales.

For the climate component, we use a two-box energy balance model. One box represents the globally averaged temperature anomaly of the atmosphere and upper ocean, T_1 (units of K), and the other represents the globally averaged temperature anomaly of the deep ocean, T_2 (K).

Radiative forcing due to a CO_2 increase heats the upper box, with a forcing due to each CO_2 doubling of $Q_{2\times}$ (Myhre et al., 1998). This logarithmic dependence means that each additional unit of CO_2 added to the atmosphere has a weaker effect than the previous.

The boxes exchange energy with each other, parametrised by a heat transfer coefficient κ , and respond to the radiative forcing caused by CO_2 , which follows the standard logarithmic form. This type of model can be fitted to the outputs of more complex Earth System Models (Cummins et al., 2020; Williamson et al., 2024) and has been shown to accurately reproduce the response to radiative forcing (Geoffroy et al., 2013).

The terrestrial carbon store, C_L (PgC), is modelled by the balance between globally averaged Net Primary Production (NPP), denoted by Π , and globally averaged heterotrophic respiration. We will neglect to explicitly represent vegetation dynamics on the assumption that the timescales of interest for the stability of the system are longer than typical vegetation timescales.

NPP is assumed to be a function of atmospheric CO_2 only. The temperature dependence of NPP is neglected, as the temperature response is weaker, at the global scale, than the CO_2 response (Varney et al., 2023). To model heterotrophic respiration we make the common assumption that it follows a Q_{10} response formula, in which respiration increases by a factor of Q_{10} for every 10 K warming. We also assume that the relevant temperature for heterotrophic respiration is the temperature over land, which is larger than global temperatures by a factor $\beta \approx 1.3$ (Byrne and O'Gorman, 2018).

Ocean carbon uptake is represented with a two box model developed by Bolin and Eriksson (1959) and Glotter et al. (2014). The boxes represent the upper and deep ocean carbon stores C_1 and C_2 (PgC), respectively, these boxes do not partition the ocean into the same way the temperature boxes do. This model accounts for changes in ocean chemistry due to increased ocean carbon. However, following Glotter et al. (2014), we neglect the role of temperature change in carbon

uptake, as this effect is smaller than the direct effect of increased CO₂ concentrations (Arora et al., 2020).

Atmospheric carbon, C_A , is required to close the model. C_A is calculated by applying conservation of mass to the total carbon in the system. Mathematically, the model can be written as:

$$c_1 \frac{\mathrm{d}T_1}{\mathrm{d}t} = -\lambda T_1 + \kappa (T_2 - T_1) + Q_{2\times} \log_2 \left(\frac{C_{\mathrm{A}}}{C_{\mathrm{A}}^*}\right) \tag{1a}$$

$$c_2 \frac{\mathrm{d}T_2}{\mathrm{d}t} = -\kappa (T_2 - T_1) \tag{1b}$$

$$\frac{\mathrm{d}C_{\mathrm{L}}}{\mathrm{d}t} = \Pi(C_{\mathrm{A}}) - \Pi\left(C_{\mathrm{A}}^{*}\right) \frac{C_{\mathrm{L}}}{C_{\mathrm{I}}^{*}} e^{\alpha\beta T_{\mathrm{I}}} \tag{1c}$$

$$\frac{dC_1}{dt} = \nu_1(C_A - \mathcal{E}(C_1)) - \nu_2 \left(C_1 - \frac{V_1}{V_2}C_2\right)$$
 (1d)

$$\frac{\mathrm{d}C_2}{\mathrm{d}t} = \nu_2 \left(C_1 - \frac{V_1}{V_2} C_2 \right),\tag{1e}$$

with carbon conservation giving

$$C_{\rm A} + C_{\rm L} + C_1 + C_2 = C_{\rm A}^* + C_{\rm L}^* + C_1^* + C_2^*,$$
 (2)

where asterisks indicate pre-industrial values.

The parameters c_1 and c_2 denote the different heat capacities of the two climate boxes. Furthermore, rather than working with ECS directly, we introduce a climate feedback parameter λ , which is related to ECS by the formula $ECS = Q_{2\times}/\lambda$.

The parameter α determines the strength of heterotrophic respiration and is related to Q_{10} by $\alpha=0.1\log Q_{10}$. The exact form of Π is not important for analytical results, as the linear stability of the pre-industrial equilibrium will only depend on $\Pi(C_A^*)$ and its derivative $\Pi'(C_A^*)$. However for numerical experiments, we assume the saturating form

$$\Pi(C_{\mathcal{A}}) = \Pi(C_{\mathcal{A}}^*) \frac{C_{\mathcal{A}}^* + C_{1/2}}{C_{\mathcal{A}}^*} \frac{C_{\mathcal{A}}}{C_{\mathcal{A}} + C_{1/2}}$$
(3)

where $C_{1/2}$ is a half-saturation constant.

The upper ocean box, with volume V_1 , absorbs carbon from the atmosphere over a fast timescale v_1^{-1} . This carbon is transported to the larger lower box, with volume V_2 , on a slower timescale, v_2^{-1} . These timescale parameters capture the effects of carbon pumps, which transport carbon to depth. We account for the effects of ocean chemistry with the function \mathcal{E} , which relates C_1 to the amount of atmospheric carbon required for equilibrium. The functional form of \mathcal{E} can be derived by assuming constant alkalinity, Alk, in the ocean. Here Alk represents carbonate alkalinity, not total alkalinity. We note that this assumption leads to lower ocean pH values than more sophisticated methods (Munhoven, 2013). The expression for \mathcal{E} is

$$\mathcal{E}(C_1) = k \left(1 + \frac{k_1}{[H^+]} + \frac{k_1 k_2}{[H^+]^2} \right)^{-1} C_1 \tag{4}$$

Parameter	Name	Value	Source
C^*_{Δ}	Pre-industrial atmospheric carbon	286.085 ppmv	JULES
$egin{array}{c} C_{ m A}^* \ C_{ m L}^* \end{array}$	Pre-industrial land carbon	1630 Pg C	JULES
$C_{1/2}^{L}$	CO ₂ fertilisation saturation constant	344 ppmv	JULES
$\Pi(C^*_{\Delta})$	Pre-industrial NPP	65 Pg C yr ⁻¹	JULES
Q_{10}	Respiration temperature sensitivity	2	Jones and Cox (2001)
κ	Heat transfer coefficient	$0.57\mathrm{W}\mathrm{m}^{-2}\mathrm{K}^{-1}$	Williamson et al. (2024)
c_1	Upper box heat capacity	$7.7\mathrm{Wm^{-2}K^{-1}yr^{-1}}$	Williamson et al. (2024)
c_2	Lower box heat capacity	$100.0\mathrm{Wm^{-2}K^{-1}yr^{-1}}$	Williamson et al. (2024)
$Q_{2 imes}$	Radiative forcing due to doubled CO ₂	$3.7{ m W}{ m m}^{-2}$	Myhre et al. (1998)
$oldsymbol{eta}$	Ratio of land to global warming	1.3	Byrne and O'Gorman (2018)
v_1	Ocean carbon uptake rate	$0.2{\rm yr}^{-1}$	Bolin and Eriksson (1959)
ν_2	Ocean carbon uptake rate	$0.002 \mathrm{yr}^{-1}$	Bolin and Eriksson (1959)
Alk	Ocean alkalinity	5130 Pg C	GCB
k	Ocean/atmosphere carbon ratio	220.0	Glotter et al. (2014)
k_1	Dissociation constant	$10^{-6} \text{mol kg}^{-1}$	Glotter et al. (2014)
k_2	Dissociation constant	$7.53 \times 10^{-10} \text{mol kg}^{-1}$	Glotter et al. (2014)

Table 1. The "default" parameter values used for the numerical evaluation of the model, unless otherwise stated. No default value is given for λ as that parameter is changed throughout the study.

where the concentration of hydrogen ions, [H⁺], can be found by solving

Ocean box volume ratio

Alk =
$$\left(\frac{k_1}{[H^+]} + \frac{2k_1k_2}{[H^+]^2}\right) \left(1 + \frac{k_1}{[H^+]} + \frac{k_1k_2}{[H^+]^2}\right)^{-1} C_1.$$
 (5)

The total amount of carbon in the system can be written as the sum of $C_{\rm L}^*,\,C_1^*,\,C_2^*,\,C_{\rm A}^*$ which are the pre-industrial carbon stores in the land, upper ocean, deep ocean and atmospheric reservoirs, respectively. Whilst $C_{\rm L}^*$ and $C_{\rm A}^*$ are free parameters of the model, the pre-industrial ocean values are calculated from the equations $C_A^* = \mathcal{E}(C_1^*)$ and $C_2^* =$ $(V_2/V_1)C_1^*$.

2.1 **Parameters**

 k_2 V_2/V_1

The parameters take the values given in Table 1, unless otherwise stated. These values mostly come from previous estimates in the literature, however some come from the output of a complex terrestrial carbon cycle model, JULES. The only parameter that we have fitted ourselves is the Alk parameter, which was chosen so that the ocean model correctly estimates the observed ocean carbon uptake over the historical period, inferred by the Global Carbon Budget (GCB) (Friedlingstein et al., 2022) (see Fig. S1 in the Supplement). We fit to the ocean uptake rather than the total ocean carbon as the response to elevated CO2 plays an important role in the system's stability. As our ocean carbon model has only two boxes, it is not suitable to accurately simulate the size of the total ocean carbon store on multi-millennial timescales.

2.2 Analysis

The pre-industrial state is an equilibrium of Eq. (1), occurring when $T_1 = T_2 = 0$, $C_A = C_A^*$, $C_L = C_L^*$, $C_1 = C_1^*$ and $C_2 = C_2^*$. Furthermore, this equilibrium exists for all parameter values.

Bolin and Eriksson (1959)

To calculate the stability of this pre-industrial equilibrium it is helpful to rewrite Eq. (1) in the condensed form

$$\frac{\mathrm{d}x}{\mathrm{d}t} = f(x) \tag{6}$$

where $\mathbf{x} = (T_1, T_2, C_1, C_1, C_2)^{\mathrm{T}}$ and \mathbf{f} is given by the righthand side of Eq. (1). Letting x^* be the pre-industrial equilibrium, we can linearise Eq. (6) about x^* to give the behaviour of small perturbations Δx

$$\frac{\mathrm{d}\Delta x}{\mathrm{d}t} = \mathbf{J}\Delta x \tag{7}$$

where the Jacobian, **J**, is given by $\mathbf{J}_{ij} = \partial f_i / \partial x_j$ evaluated at x^* .

At large t, the perturbation will be dominated by a contribution along the fastest growing (or slowest decaying) direction in phase space, which is the space of possible states of the system. Mathematically, as $t \to \infty$, the perturbation behaves like $\Delta x(t) \sim c_{\rm m} v_{\rm m} \exp(\gamma_{\rm m} t)$ where $\gamma_{\rm m}$ is the eigenvalue of **J** with the largest real part, $v_{\rm m}$ the corresponding eigenvector and $c_{\rm m}$ a constant given by the initial conditions. If $\text{Re}\gamma_{\text{m}} > 0$, the perturbation grows and therefore the equilibrium is unstable. If $Re\gamma_m < 0$ the perturbation decays and so the equilibrium is stable.

Therefore we must determine when the eigenvalues of **J** have zero real part to find the critical parameters for which the stability of the pre-industrial equilibrium changes. Evaluated at the pre-industrial equilibrium, **J** is

$$\mathbf{J} = \begin{bmatrix} -\frac{\lambda + \kappa}{c_1} & \frac{\kappa}{c_1} & -\frac{Q_{2\times}}{c_1 C_A^* \log 2} & -\frac{Q_{2\times}}{c_1 C_A^* \log 2} & -\frac{Q_{2\times}}{c_1 C_A^* \log 2} \\ \frac{\kappa}{c_2} & -\frac{\kappa}{c_2} & 0 & 0 & 0 \\ -\alpha \beta \Pi(C_A^*) & 0 & -\frac{d\Pi}{dC_A} - \frac{\Pi(C_A^*)}{C_L^*} & -\frac{d\Pi}{dC_A} & -\frac{d\Pi}{dC_A} \\ 0 & 0 & -\nu_1 & -\nu_1 (1 + \mathcal{E}'(C_1^*)) - \nu_2 - \nu_1 + \frac{\nu_1}{\nu_2} \nu_2 \\ 0 & 0 & 0 & \nu_2 & -\frac{\nu_1}{\nu_2} \nu_2 \end{bmatrix}$$
(8)

where \mathcal{E}' denotes the derivative of \mathcal{E} with respect to C_1 . The eigenvalues, γ , of the Jacobian satisfy the characteristic equation, $\det(\mathbf{J} - \gamma \mathbf{I}) = 0$ giving

$$\gamma^5 + p_4 \gamma^4 + p_3 \gamma^3 + p_2 \gamma^2 + p_1 \gamma + p_0 = 0, \tag{9}$$

where $\{p_i\}$ are functions of the parameters of the model.

Ideally, we would solve Eq. (9) for γ and would then find the critical parameter values for which $\text{Re}\gamma=0$. However, because Eq. (9) is a quintic polynomial, no general solution exists. Therefore, we must rely on special cases and approximations to make progress.

A simple case occurs when γ is purely real. In that case, $\gamma = 0$ is a solution when $p_0 = 0$. When $p_0 = 0$, The parameters satisfy

$$\frac{\alpha\beta Q_{2\times}}{\lambda \log 2} = \frac{V_2}{V_1} \frac{\text{d} \log \Pi}{\text{d} \log C_A} + \frac{C_A^*}{C_L^*} \left(1 + \frac{1}{\mathcal{E}'} + \frac{1}{\mathcal{E}'} \frac{V_2}{V_1} \right). \tag{10}$$

The bifurcation this corresponds to can be shown to be a transcritical bifurcation, in which a new stable steady state emerges near to the old, now unstable, steady state.

If γ has non-zero imaginary part, exact results cannot be obtained. However, because we are interested in γ values near the bifurcation, we can guarantee that $\text{Re}\gamma$ is small. Making the further assumption that $\text{Im}\gamma$ is small means that cubic terms and higher can be dropped from Eq. (9). The resulting quadratic equation can be solved to give

$$\operatorname{Re}\gamma \approx -\frac{p_1}{2p_2},\tag{11}$$

which in terms of the climate feedback parameter, λ , can be written as

$$\operatorname{Re}\gamma \approx \frac{\lambda + g_1}{g_2\lambda + g_3},\tag{12}$$

where $\{g_i\}$ are functions of the parameters.

Setting this growth rate equal to zero gives an expression for the critical λ , which is given in the Supplement as Eq. (S1). The resulting equation is too complicated to be useful; however further approximations can be made to make it tractable. As the deep ocean is much larger and absorbs carbon over a slower timescale than the upper ocean, it can be assumed that $\mathcal{E}'\nu_1 \gg \nu_2$, $\nu_1 \gg \nu_2$, $c_2 \gg c_1$ and $V_2 \gg V_1$. In this approximation, the equation reduces to

$$\frac{\alpha\beta Q_{2\times}}{\lambda \log 2} = \left(\frac{\mathrm{d}\log\Pi}{\mathrm{d}\log C_{\mathrm{A}}} + \frac{C_{\mathrm{A}}^*}{C_{\mathrm{L}}^*} \left(1 + \frac{1}{\mathcal{E}'} + \frac{c_2\nu_2}{\kappa\mathcal{E}'} + \frac{C_{\mathrm{L}}^*\nu_2}{\Pi_0\mathcal{E}'}\right)\right) \times \left(1 + \frac{C_{\mathrm{A}}^*\nu_2c_2}{C_{\mathrm{L}}^*\mathcal{E}'\alpha\beta Q_{2\times}}\right). \tag{13}$$

As γ is purely imaginary, this corresponds to a Hopf bifurcation, which means the system transitions from a steady state to an oscillatory state.

It should be noted that Eq. (10) contains factors of V_2/V_1 whereas Eq. (13) does not. The deep ocean is much larger than the upper ocean, $V_2 \gg V_1$. This means that the transcritical bifurcation occurs at much higher values of ECS than the Hopf bifurcation does. Therefore, we will focus on the Hopf bifurcation in the rest of the study.

The approximate expression for the critical climate sensitivity, Eq. (13), was verified by numerically calculating the growth rate from the Jacobian, **J**, and identifying where it is zero. This numerical result was compared to Eq. (13) for a range of ECS and CO2 fertilisation strengths, and for three different C_{Λ}^* values. Although C_{Λ}^* was introduced as the amount of carbon stored in the pre-industrial atmosphere, we can generalise this to the case where C_{Λ}^* represents a potential atmospheric carbon steady state, and measure temperature anomalies relative to the global temperatures the value of C_A^* implies. We can then determine how stable or unstable that state would be. This allows us to consider how the amount of carbon in the atmosphere affects the stability of the system. These C_A^* values correspond to the pre-industrial equilibrium, a doubling of CO_2 and $C_A^* = 190$ ppmv which was the atmospheric CO₂ level during at Last Glacial Maximum (LGM) (Kageyama et al., 2017).

The results are shown in Fig. 2. The figure shows the numerically determined growth rates, as well as the approximation Eq. (13). The approximation gives good agreement with the numerically determined values, supporting the usefulness of the approximation Eq. (13) across a range of parameter values.

It is worth dwelling on the meaning of the individual terms in Eq. (13). The left-hand side of the equation consists of a product of two sensitivities. One sensitivity in the product is $Q_{2\times}/\lambda = \text{ECS}$, which is the sensitivity of global temperatures to atmospheric carbon. The other sensitivity is the sensitivity of respiration to increased land temperatures, $\alpha\beta$. These are the two ingredients in the positive feedback loop between global temperatures and respiration. The two factors do not enter Eq. (13) on totally equal terms, however, as a factor of $\alpha\beta$ also appears on the right-hand side of the equation.

The right-hand side of Eq. (13) consists of negative feed-backs which stabilise the climate–carbon system. The first of these is $d \log \Pi/d \log C_A$, which measures the magnitude of the CO_2 fertilisation effect. The larger this is, the more stable the system becomes. The next term is a factor in parentheses multiplied by the ratio C_A^*/C_L^* . This ratio implies that the greater the proportion of carbon held in the atmosphere relative to land the more stable the system is. This effect can be attributed to the fact that heterotrophic respiration increases linearly with land carbon but radiative forcing increases only logarithmically with CO_2 . As it is the ratio, rather than the sum, of carbon stored in the atmosphere to carbon stored in

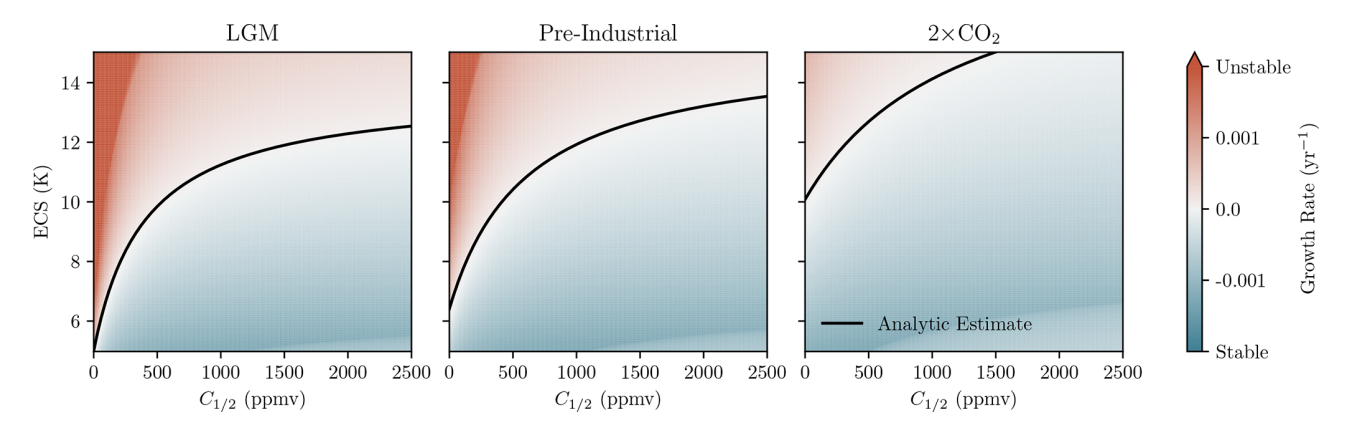


Figure 2. Growth rates of perturbations to the equilibrium state in the conceptual model, Eq. (1), for a range of ECS, CO₂ fertilisation effect strengths, and different atmospheric carbon levels. The colours correspond to growth rates calculated numerically and the solid line is given by Eq. (13). This line agrees with the numerics as to when the growth rate is zero.

the land that appears in Eq. (13), the stability of the system does not depend straightforwardly on the total carbon store.

The factor in parentheses is a sum of timescale ratios. The timescales are: κ/c_2 (ocean heat uptake timescale), ν_2^{-1} (deep ocean carbon uptake timescale) and C_L^*/Π_0 (soil carbon turnover time). They imply that the system is less stable if the ocean absorbs carbon slowly relative to the time the ocean takes to warm or if carbon cycles quickly through the soil compared to the ocean. Each of these timescale ratios is multiplied by \mathcal{E}'^{-1} , which describes how a change in ocean carbon affects the air-sea carbon equilibrium. If this value is large, the ocean absorbs more carbon for a given change in atmospheric concentration, which acts to stabilise the system.

2.3 Numerical results

We performed numerical experiments to analyse the behaviour of the model around the bifurcation. We initialised the system near the pre-industrial equilibrium by increasing atmospheric carbon by 20 ppmv and integrating for 50 000 years. This is a longer timescales than the model is strictly valid for, however it gives enough time to show the system's dynamics.

Figure 3 shows the resulting atmospheric CO₂ time series for ECS values of 3, 6 and 12 K. Additionally, we repeated the experiment in the case when the CO₂ fertilisation effect was absent. When the CO₂ effect was present, the cases where the ECS was 3 or 6 K relaxed back to equilibrium; these parameters correspond to a stable equilibrium. However, for an ECS of 12 K the system approaches a limit cycle. Between these ECS values the system passed through a Hopf bifurcation, causing the pre-industrial state to become unstable.

A projection of the C_A - C_L plane is shown in Fig. 3. It shows that the limit cycle involves moving large quantities of carbon between the land and the atmosphere. It should be

noted that the amplitude and period of this limit cycle are large enough that the system has been pushed into a regime where the assumptions in the model are no longer strictly valid.

The limit cycle emerges because carbon is transferred back and forth between the land and the atmosphere. When there are sufficient stocks of terrestrial carbon, the positive feedback between heterotrophic respiration and global warming moves carbon from the land to the atmosphere. As there is now less carbon in the land, heterotrophic respiration decreases and, due to the CO₂ fertilisation effect, NPP increases. This means that carbon now instead flows back into the land from the atmosphere, and so the cycle can begin again.

The result of turning off the CO_2 fertilisation effect (i.e. setting $C_{1/2}$ to zero) is shown in the bottom row of Fig. 3. In this case, the pre-industrial state becomes unstable at lower values of ECS. In particular instability occurs for an ECS of 6 K. Furthermore, the instability is more serious in that the system diverges rather than approaches a limit cycle. This represents a deficiency the model, arising from not accounting for effects that occur at low CO_2 .

A more systematic investigation of the system's behaviour can be performed by plotting the system's equilibrium state against a varying parameter, known as a bifurcation diagram. Figure 4 shows a bifurcation diagram of atmospheric carbon as a function of ECS for the cases with and without a CO_2 fertilisation effect, computed by the XPP-AUTO continuation software (Ermentrout, 2002). Figure 4 shows that, with a CO_2 fertilisation effect, above a critical climate sensitivity of $10.9 \, \text{K}$, the pre-industrial state is unstable. Beyond this threshold, the system undergoes a Hopf bifurcation and develops large oscillations in the CO_2 levels. When the CO_2 fertilisation effect is absent, the bifurcation occurs at a lower ECS of just below $6 \, \text{K}$. The Hopf bifurcation is supercritical (a stable oscillation exists after the bifurcation) in the first case but subcritical (an unstable oscillation exists

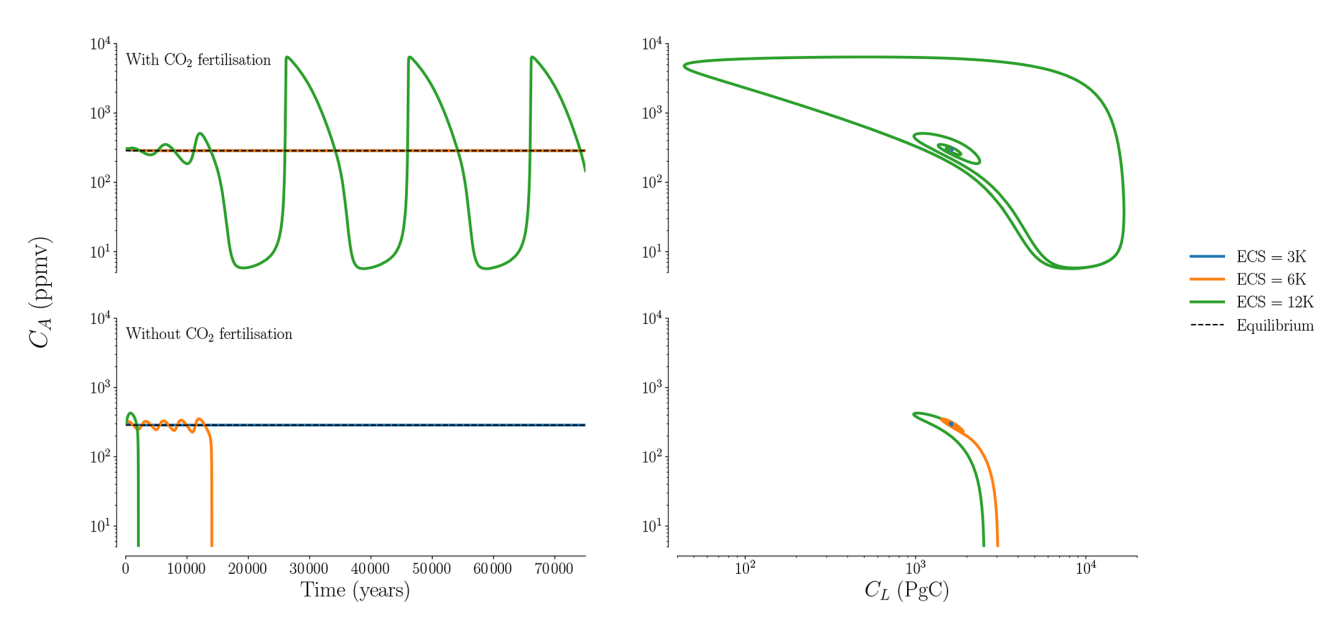


Figure 3. The response of Eq. (1) to a small 20 ppmv perturbation to CO_2 when the ECS is 3, 6 or 12 K and the CO_2 fertilisation effect is either present (top row, $C_{1/2} = 344$ ppmv) or absent (bottom row, $C_{1/2} = 0$ ppmv). The left column shows a time series of atmospheric carbon and the right shows the trajectories projected onto the C_A - C_L plane.

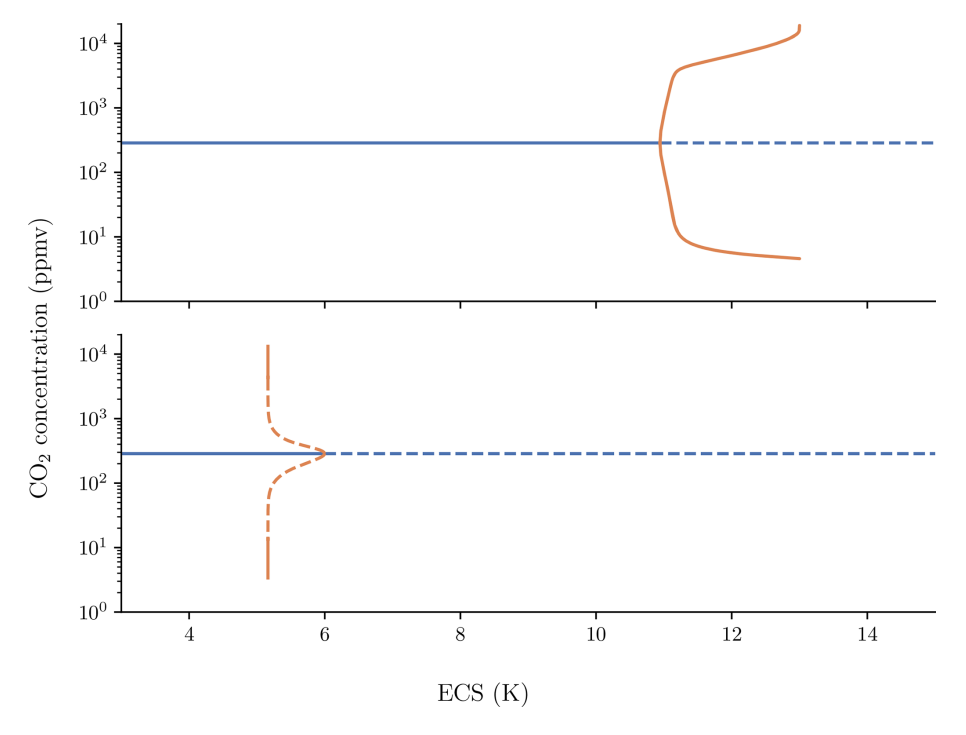


Figure 4. A bifurcation diagram for Eq. (1), showing the equilibrium behaviour of atmospheric carbon as a function of climate sensitivity with a CO_2 fertilisation effect (top) and without (bottom). The blue solid line indicates a stable fixed point, corresponding to the pre-industrial state. The dashed line indicates an unstable fixed point and the orange curves show the maximum and minimum values of the limit cycle.

before the bifurcation) in the second case. This explains why the system diverged in some of the numerical experiments plotted in Fig. 3.

The dependence on the CO₂ fertilisation effect strength and pre-industrial CO₂ levels were further investigated, by

numerically solving for the eigenvalues of the Jacobian, which are the solutions to Eq. (9). Figure 5 shows the dependence of the critical ECS value on $C_{1/2}$ and $C_{\rm A}^*$ for $Q_{10}=2$ and $Q_{10}=3$. As $C_{\rm A}^*$ increases, the critical ECS does too. This indicates that the system is more stable at high CO₂ lev-

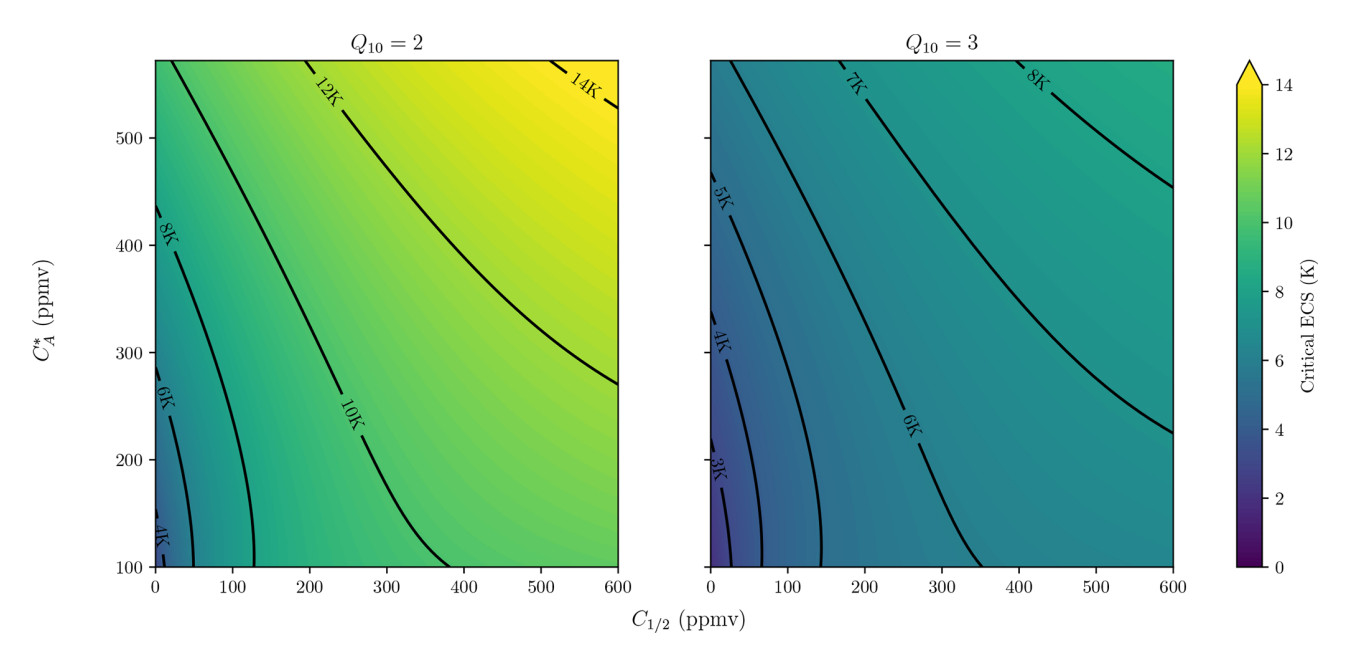


Figure 5. The critical ECS as a function of CO_2 levels, C_A^* , and the CO_2 fertilisation effect for two different values of Q_{10} . Notice the critical ECS is smaller for smaller pre-industrial CO_2 levels, CO_2 fertilisation strength and larger Q_{10} .

els and therefore anthropogenic CO_2 emissions are unlikely to trigger this instability. Furthermore as the strength of the CO_2 fertilisation effect decreases, the system is unstable at lower ECS values.

When $Q_{10} = 2$, Fig. 5 shows that the critical ECS enters the range of CMIP6 models (i.e. less than 6 K) for weak CO_2 fertilisation effects and low CO_2 levels, a regime relevant to the Last Glacial Maximum. If $Q_{10} = 3$ then the critical ECS becomes comparable to the ECS of CMIP6 models, even for a comparatively strong CO_2 fertilisation effect at low enough CO_2 levels.

3 Complex model

Equation (1) is, by construction, a significant simplification of the real Earth system, which has many more processes and is spatially heterogeneous. This is important, for example, as warming caused by increased atmospheric CO₂ is also spatially heterogeneous; the poles warm faster than equatorial regions (Huntingford and Mercado, 2016). To avoid the limitations of the simple model, we examine the results from a complex land surface model, the Joint UK Land Environmental Simulator (JULES) (Best et al., 2011; Clark et al., 2011).

3.1 Model description

JULES is a state-of-the-art model of land-atmosphere exchanges of momentum, water and vapour, and fluxes of carbon. JULES has a dynamic vegetation component (TRIF-FID) and a RothC four-pool model of soil carbon, operating

at a spatial resolution of $2.5^{\circ} \times 3.75^{\circ}$. JULES is driven by meteorological forcings from a model called the Integrated Model Of Global Effects of climatic aNomalies (IMOGEN), which includes carbon cycle feedbacks on atmospheric and ocean carbon.

IMOGEN is a spatially-explicit intermediate complexity model (Huntingford et al., 2010) which is coupled to the JULES land surface model at the same spatial resolution. IMOGEN provides spatially-explicit meteorological forcings to drive JULES and dynamically responds to changes in CO₂. The response to CO₂ is estimated using pattern scaling, which assumes that the change in some spatially-resolved meteorological variable ΔX at location r, year t, and month m can be written as $\Delta X(r,t,m) = p(r,m)\overline{\Delta T}(t)$ where p is a spatial pattern and $\overline{\Delta T}$ is global mean temperature change. The temperature change is determined by an energy balance model with ocean heat uptake parametrised diffusively. The pattern and energy balance model parameters are fitted to the actual patterns of change projected by different ESMs. In this way, IMOGEN can emulate different ESMs (Huntingford et al., 2000). In this study, we use IMOGEN to create an emulator of the HadGEM2-ES model (Jones et al., 2011).

To close the global carbon cycle, IMOGEN also provides a model for ocean carbon uptake based on the impulse-response formulation given by Joos et al. (1996), which was calibrated to match the behaviour of process-based models. Uptake of carbon by the oceans in IMOGEN depends both on ocean temperatures and atmospheric CO₂ concentrations.

JULES and IMOGEN are fully coupled. IMOGEN provides JULES with meteorological forcing, which affects the terrestrial carbon cycle modelled by JULES. JULES then

provides land-atmosphere carbon fluxes to IMOGEN, as the terrestrial land stores evolve. IMOGEN combines this flux with the ocean-atmosphere carbon flux to update atmospheric CO₂, which leads to changes in climate and thus feeds back to the meteorological forcing given to JULES.

3.2 Experimental configuration

For this study, we took advantage of the fact that the ECS of IMOGEN can be set explicitly. This means that we can run multiple experiments varying the ECS values to determine which value of ECS leads to an instability of the preindustrial state.

To initialise JULES in a pre-industrial equilibrium state, the JULES/IMOGEN system was run with a prescribed constant concentration of atmospheric carbon and no ocean carbon uptake. As IMOGEN is an anomaly model, calculating changes relative to a given climatology, the equilibrium state is not a function of ECS. As a result, only one initialisation was required. JULES was run until the slowest carbon stores (namely the soil pools) reached an approximate steady state. To verify that an approximate steady state had been reached, a further 600 years of simulation was performed, and the change in soil carbon was found to be 0.008 % over this period, suggesting a near-equilibrium state (also see Fig. S3 in the Supplement).

Once this approximate steady state had been reached, atmospheric carbon was increased by 2 ppmv and 13 different simulations were run, each with a different ECS. In these simulations, ocean carbon uptake was enabled, and atmospheric carbon was allowed to change dynamically. The simulations lasted 5000 years; longer integrations were ruled out due to computational limitations. After an initial transient of 250 years, the change in CO₂ was assumed to follow the form $\Delta C_{\rm A}(t) \propto e^{\gamma_{\rm m}t}$. A linear fit to the logarithm of this growth was used to find the growth rate. The sign of γ determines the stability of the pre-industrial state: positive values indicate instability and negative indicate stability.

3.3 Results

The results of this experiment are plotted in Fig. 6. The figure shows the changing CO₂ levels for different values of ECS. CO₂ levels show exponential change over a millennial timescale. The CO₂ changes are all consistent with exponential growth or decay, although it is possible we are detecting a very long period oscillation. For large enough ECS values, there is exponential growth, indicating an unstable steady state, but for smaller values of ECS the system undergoes exponential decay, indicating a stable steady state. The growth rates, given by the slopes of these lines, are plotted in Fig. 7 against ECS.

Figure 7 shows the growth rates of atmospheric CO_2 as a function of ECS. The curve given by Eq. (12) was fitted to this data to enable estimation of the critical ECS value, which

occurs when the growth rate is 0. The critical ECS value was found to be $10.9\pm0.6\,\mathrm{K}$, where the uncertainty is given by a 95 % confidence interval. This compares remarkably well with the prediction of the simple model, with the central estimate matching its prediction.

This unstable growth in JULES/IMOGEN is associated with a decrease in global soil carbon (see Fig. S4 in the Supplement). Furthermore, soil carbon and heterotrophic respiration in JULES are modelled in a similar way to how we have modelled them in the simple model, suggesting that the instability in IMOGEN/JULES and the instability in the simple model share a common mechanism. Furthermore, the agreement between the simple and complex model on the critical ECS value suggest that the simple model captures the relevant processes needed to determine the stability of the climate—carbon system.

4 Discussion and conclusions

In this paper, we examined the conditions under which the positive feedback loop between heterotrophic respiration and global warming could lead to an unstable, runaway growth in atmospheric CO₂. We examined a simple conceptual model of the climate–carbon cycle system to explain this mechanism. To test the results of the simple model, we performed experiments with the coupled climate–carbon model JULES/IMOGEN.

Using the parameters in Table 1, the simple model predicts that the pre-industrial climate—carbon state can undergo a Hopf bifurcation. We were able to derive a formula for the critical parameters at which this bifurcation occurs. In particular the simple model is unstable for equilibrium climate sensitivities above 10.9 K. This critical value is outside the likely range of ECS of 2.6–3.9 K (Sherwood et al., 2020), which is consistent with the observed stability of pre-industrial climate—carbon cycle state.

The parameters in Table 1 are generally realistic, as they are based on the outputs of complex models that reproduce observed climate change. The main exception however is our choice of the alkalinity, Alk. We have an unrealistically high value, which leads to too much carbon stored in the ocean. A lower, more realistic, choice of Alk would tend to make the system less stable as it would reduce the ocean's ability to take up carbon. However, a lower choice of Alk would mean that the ocean model could not reproduce the observed change in ocean carbon over the historical period.

Some unrealistic assumptions were made about the climate–carbon system. For example, we neglected the effect of temperature change on NPP and CO₂ solubility, which tends to destabilise the system. Furthermore, we ignored spatial heterogeneity and assumed two boxes were sufficient to capture the climate response, although in fact three may be optimal (Cummins et al., 2020). These unrealistic assumptions are particularly acute after the Hopf bifurcation where

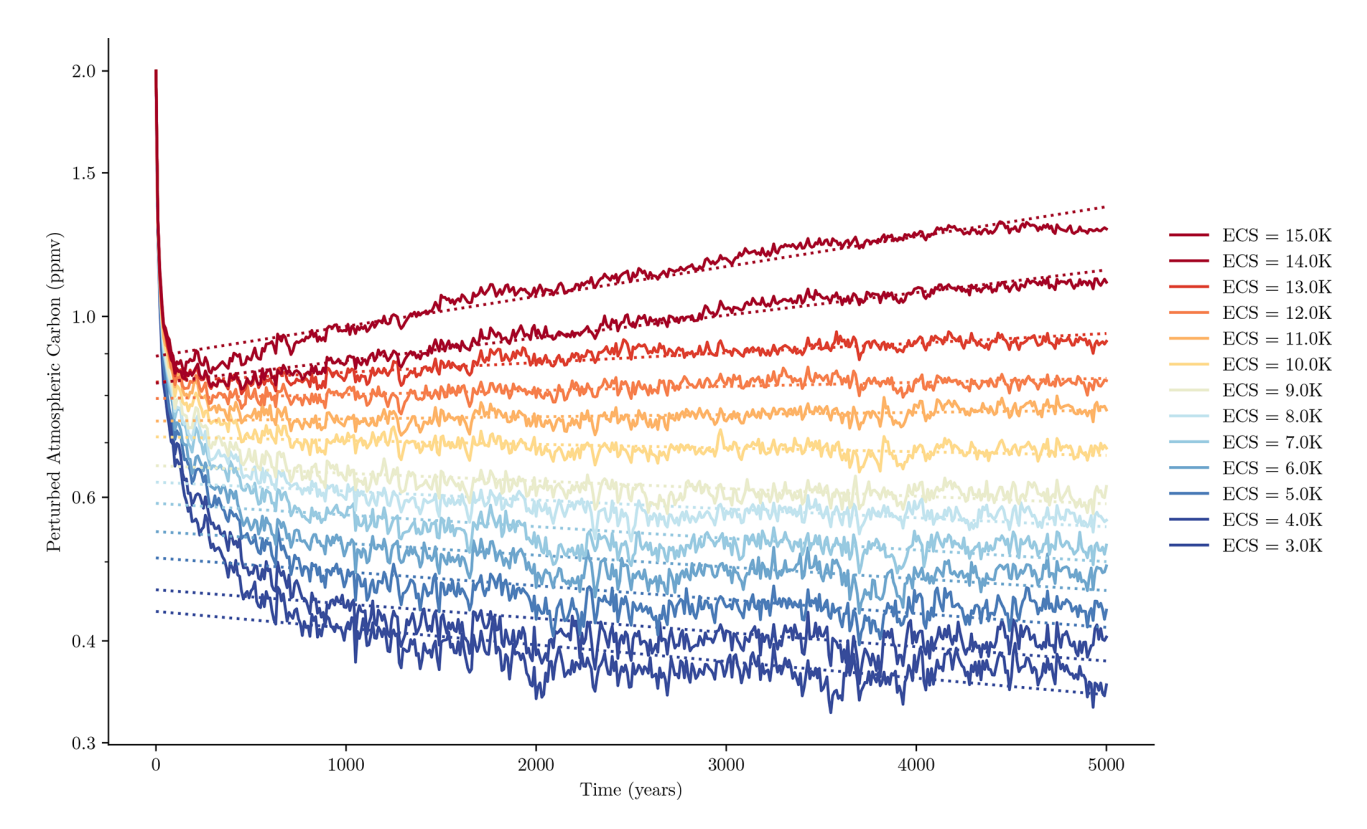


Figure 6. Atmospheric CO₂ from a JULES run for a variety of different climate sensitives. The system was initialised from an equilibrium state and given a perturbation of 2 ppmv of CO₂. After an initial transient the atmospheric CO₂ changes exponentially with time, which corresponds to a linear change on a logarithmic scale. In dotted lines we plot fits of exponential growth or decay to the latter portion of the time series. As ECS increases, the system transitions from stable exponential decay to unstable exponential growth.

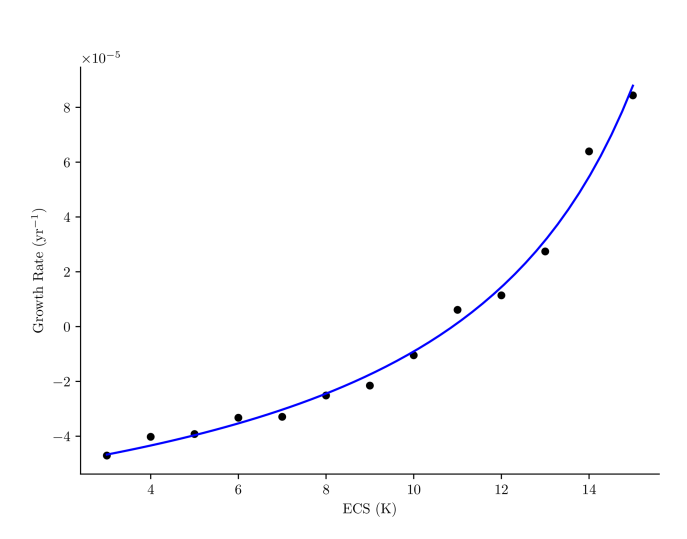


Figure 7. The growth rates of CO_2 as estimated from the time series shown in Fig. 6. Fitting Eq. (12) gives the blue line. The *x*-intercept gives the critical ECS at which the bifurcation occurs. The estimated critical ECS is 10.9 ± 0.6 K.

the limit cycle pushes the system into extreme regions of phase space (such as at very high or very low CO_2).

We were also able to use the JULES/IMOGEN model to estimate the critical equilibrium climate sensitivity which leads to instability, which was also determined to be around 10.9 K. Unlike the simple model, this model does not neglect temperature feedbacks on NPP or ocean carbon uptake. Furthermore it is fully spatially resolved, and does not make unrealistic assumptions about the alkalinity of the ocean. However, due to computational constraints we are not able to run JULES/IMOGEN for long enough to see what state the model tends to after the instability. Furthermore, we were not able to run the model for long enough to determine whether the increase in CO₂ is a genuine instability or just the start of a decaying oscillation.

Both modelling approaches have complementary strengths and weaknesses. The qualitative agreement between the models (an instability occurring around 11 K driven by heterotrophic respiration) therefore indicates a robustness to our conclusions.

That climate–carbon instability can play a role in Earth system, specifically paleoclimate, dynamics has long been appreciated. For example Saltzman and Maasch (1988) showed how unstable interactions between physical climate

and ocean carbon uptake could lead to oscillations resembling the Pleistocene glacial-interglacial cycles. More recently, Boot et al. (2022) showed how ocean circulation can induce a Hopf bifurcation in the carbon cycle, potentially explaining some CO₂ variability. On longer timescales, Hülse and Ridgwell (2025) demonstrated that different carbon cycle processes could "out-compete" the silicate weathering thermostat, leading to significant cooling. The carbon cycle may also be excitable (Rothman, 2019), meaning small perturbations lead to large responses. Extreme fluctuations can be seen in isotopic records which show a heavy-tailed distribution (Arnscheidt and Rothman, 2021). Carbon cycle instability can even be seen in high CO₂ exoplanets (Graham and Pierrehumbert, 2024). This paper (and Cox et al., 2006) is unusual in that it studies an instability in the interaction of the terrestrial biosphere with the physical climate.

Although our analysis has focused on the pre-industrial climate–carbon equilibrium, we can apply our results to a wider range of climate–carbon cycle states. We must be working on timescales long enough that there is a steady state CO_2 concentration, C_A^* , to which the climate–carbon system has equilibrated but short enough that astronomical forcing and carbon cycle changes due to silicate weathering can be neglected.

For example, we may consider a future climate state with elevated CO₂ levels caused by anthropogenic emissions. Perhaps counter-intuitively, this state may be more stable than the pre-industrial climate as the critical ECS scales with atmospheric carbon.

Conversely, climate—carbon states with lower atmospheric carbon, for example at the Last Glacial Maximum (LGM), are less stable. The size of the CO₂ fertilisation effect differs across CMIP6 ESMs, although the JULES prediction is close to the ensemble mean (Varney et al., 2023). We find that if CO₂ fertilisation of photosynthesis is negligible, perhaps due to strong nitrogen limitations, then the LGM state is unstable for a critical ECS of 4.5 K, which is within the CMIP6 range. This instability may manifest, as it does in the JULES/IMOGEN run, as a continual drift in atmospheric CO₂ concentrations.

It is natural to ask if any CMIP6 models are unstable. Whilst it is possible that modelling groups may "tune away" this instability, it may persist in other models. One reason may be that this instability occurs slowly, so it may not be detectable over the typical duration ESMs are run for. More fundamentally, the most widely used CMIP experiments (such as piControl, 1pctCO2, abrupt-4xCO2, historical and the SSP scenarios) are forced with prescribed concentrations of CO2, rather than dynamically updating CO2 concentrations due to the carbon cycle. This cuts the feedback loop between warming and respiration. Therefore, even if ESMs were unstable, this would not be apparent in typical CMIP simulations.

However, there is a push to run CMIP7 ESMs with dynamically updated CO₂ (Sanderson et al., 2024). If the CMIP7

ensemble, like CMIP6, continues to include ESMs with a large climate sensitivities then it is possible the climate-carbon instability may arise. Although our central parameter estimates give a critical ECS of 10.9 K for the pre-industrial state, we find that if the CO₂ fertilisation effect is weak enough then the critical ECS becomes 6 K, just on the edge of the CMIP6 range. However we expect models in an LGM configuration to be unstable at even lower climate sensitivities.

In summary, we have examined the possibility of an instability within the climate—carbon system. This instability is caused by a positive feedback loop between global temperatures and heterotrophic respiration. We find that this instability can only occur for sufficiently high ECS. Our analysis suggests that the high ECS values of some ESMs combined with a weak CO₂ fertilisation effect may not be compatible with a stable glacial climate.

Code and data availability. Code and data used in this paper can be found at https://doi.org/10.5281/zenodo.17640187 (Clarke, 2025). The JULES code used in these simulations is available from the Met Office Science Repository Service (registration required) at https://code.metoffice.gov.uk/trac/jules (last access: 29 July 2025). The suite used is u-dr675 and available (registration required) at https://code.metoffice.gov.uk/trac/roses-u (last access: 29 July 2025).

Supplement. The supplement related to this article is available online at https://doi.org/10.5194/esd-16-2087-2025-supplement.

Author contributions. JC analysed the simple model and JULES runs as well as producing the figures. PDLR performed the continuation analysis. MS and RV helped parametrise the model. CH helped with performing long integrations with JULES/IMO-GEN. PC conceptualised the study. All authors helped with interpreting the results and drafting the paper.

Competing interests. The contact author has declared that none of the authors has any competing interests.

Disclaimer. Publisher's note: Copernicus Publications remains neutral with regard to jurisdictional claims made in the text, published maps, institutional affiliations, or any other geographical representation in this paper. While Copernicus Publications makes every effort to include appropriate place names, the final responsibility lies with the authors. Views expressed in the text are those of the authors and do not necessarily reflect the views of the publisher.

Acknowledgements. Joseph Clarke is grateful to Eleanor Burke for assistance with setting up JULES/IMOGEN. Paul D. L. Ritchie and Peter Cox acknowledge support from the European Union's

Horizon Europe research and innovation programme under grant agreement No. 101137601 (ClimTip): Funded by the European Union. Paul D. L. Ritchie, Peter Cox, Mark Williamson and Chris Huntingford acknowledge support from the UK Advanced Research and Invention Agency (ARIA) via the project "AdvanTip". Joseph Clarke, Chris Huntingford and Peter Cox acknowledge support from the PREDICT project which has received funding from the European Space Agency (ESA) under ESA Contract No. 4000146344/24/I-LR. RV acknowledges support from Schmidt Sciences through the CALIPSO project.

Financial support. This research has been supported by the European Space Agency (PREDICT grant), the HORIZON EUROPE European Research Council (ClimTip grant), AdvantTip (grant no. SCOP-PR01-P003 – Advancing Tipping Point Early Warning AdvanTip), and CALIPSO.

Review statement. This paper was edited by Ben Kravitz and reviewed by Amber Boot and one anonymous referee.

References

- Arnscheidt, C. W. and Rothman, D. H.: Asymmetry of extreme Cenozoic climate–carbon cycle events, Science Advances, 7, eabg6864, https://doi.org/10.1126/sciadv.abg6864, 2021.
- Arora, V. K., Katavouta, A., Williams, R. G., Jones, C. D., Brovkin, V., Friedlingstein, P., Schwinger, J., Bopp, L., Boucher, O., Cadule, P., Chamberlain, M. A., Christian, J. R., Delire, C., Fisher, R. A., Hajima, T., Ilyina, T., Joetzjer, E., Kawamiya, M., Koven, C. D., Krasting, J. P., Law, R. M., Lawrence, D. M., Lenton, A., Lindsay, K., Pongratz, J., Raddatz, T., Séférian, R., Tachiiri, K., Tjiputra, J. F., Wiltshire, A., Wu, T., and Ziehn, T.: Carbonconcentration and carbon-climate feedbacks in CMIP6 models and their comparison to CMIP5 models, Biogeosciences, 17, 4173–4222, https://doi.org/10.5194/bg-17-4173-2020, 2020.
- Best, M. J., Pryor, M., Clark, D. B., Rooney, G. G., Essery, R. L. H., Ménard, C. B., Edwards, J. M., Hendry, M. A., Porson, A., Gedney, N., Mercado, L. M., Sitch, S., Blyth, E., Boucher, O., Cox, P. M., Grimmond, C. S. B., and Harding, R. J.: The Joint UK Land Environment Simulator (JULES), model description Part 1: Energy and water fluxes, Geosci. Model Dev., 4, 677–699, https://doi.org/10.5194/gmd-4-677-2011, 2011.
- Bolin, B. and Eriksson, E.: Distribution of matter in the sea and the atmosphere, The Atmosphere and the Sea in Motion, ROCKE-FELLER INSTITUTE PRESS, 130–142, 1959.
- Boot, A., von der Heydt, A. S., and Dijkstra, H. A.: Effect of the Atlantic Meridional Overturning Circulation on atmospheric *p*CO₂ variations, Earth Syst. Dynam., 13, 1041–1058, https://doi.org/10.5194/esd-13-1041-2022, 2022.
- Byrne, M. P. and O'Gorman, P. A.: Trends in continental temperature and humidity directly linked to ocean warming, Proceedings of the National Academy of Sciences, 115, 4863–4868, https://doi.org/10.1073/pnas.1722312115, 2018.
- Canadell, J. G., Monteiro, P. M. S., Costa, M. H., da Cunha, L., Cox, P. M., Eliseev, A. V., Henson, S., Ishii, M., Jaccard, S., Koven, C., Lohila, A., Patra, P. K., Piao, S., Rogelj, J.,

- Syampungani, S., Zaehle, S., and Zickfeld, K.: Global Carbon and Other Biogeochemical Cycles and Feedbacks, in: Climate Change 2021 The Physical Science Basis, edited by: Masson-Delmotte, V., Zhai, P., Pirani, A., Connors, S. L., Péan, C., Berger, S., Caud, N., Chen, Y., Goldfarb, L., Gomis, M. I., Huang, M., Leitzell, K., Lonnoy, E., Matthews, J. B. R., Maycock, T. K., Waterfield, T., Yelekçi, O., Yu, R., and Zhou, B., Cambridge University Press, Cambridge, UK and New York, NY, USA, https://doi.org/10.1017/9781009157896.007, pp. 673–816, 2021.
- Chen, D., Rojas, M., Samset, B., Cobb, K., Diongue Niang, A., Edwards, P., Emori, S., Faria, S., Hawkins, E., Hope, P., Huybrechts, P., Meinshausen, M., Mustafa, S., Plattner, G.-K., and Tréguier, A.-M.: Framing, context, and methods, in: Climate change 2021: The physical science basis. Contribution of working group I to the sixth assessment report of the intergovernmental panel on climate change, edited by: Masson-Delmotte, V., Zhai, P., Pirani, A., Connors, S. L., Péan, C., Berger, S., Caud, N., Chen, Y., Goldfarb, L., Gomis, M. I., Huang, M., Leitzell, K., Lonnoy, E., Matthews, J. B. R., Maycock, T. K., Waterfield, T., Yelekçi, O., Yu, R., and Zhou, B., Cambridge University Press, Cambridge, UK and New York, NY, USA, https://doi.org/10.1017/9781009157896.003, pp. 147–286, 2021.
- Clarke, J.: josephjclarke/Climate-Carbon-Instability: Published Release, Zenodo [data set], https://doi.org/10.5281/zenodo.17640187, 2025.
- Clark, D. B., Mercado, L. M., Sitch, S., Jones, C. D., Gedney, N., Best, M. J., Pryor, M., Rooney, G. G., Essery, R. L. H., Blyth, E., Boucher, O., Harding, R. J., Huntingford, C., and Cox, P. M.: The Joint UK Land Environment Simulator (JULES), model description Part 2: Carbon fluxes and vegetation dynamics, Geosci. Model Dev., 4, 701–722, https://doi.org/10.5194/gmd-4-701-2011, 2011.
- Cox, P. M., Betts, R. A., Jones, C. D., Spall, S. A., and Totter-dell, I. J.: Acceleration of global warming due to carbon-cycle feedbacks in a coupled climate model, Nature, 408, 184–187, https://doi.org/10.1038/35041539, publisher: Nature Publishing Group, 2000.
- Cox, P. M., Huntingford, C., and Jones, C. D.: Conditions for sink-to-source transitions and runaway feedbacks from the land carbon cycle, in: Avoiding Dangerous Climate Change, edited by: Schellnhuber, H. J., Cramer, W., Nakicenovic, N., and Wigley, T., Cambridge University Press, https://ore.exeter.ac.uk/repository/handle/10036/48545 (last access: 30 July 2025), 2006.
- Cummins, D. P., Stephenson, D. B., and Stott, P. A.: Optimal Estimation of Stochastic Energy Balance Model Parameters, Journal of Climate, 33, 7909–7926, https://doi.org/10.1175/JCLI-D-19-0589.1, 2020.
- Davidson, E. A. and Janssens, I. A.: Temperature sensitivity of soil carbon decomposition and feedbacks to climate change, Nature, 440, https://doi.org/10.1038/nature04514, 2006.
- DeVries, T.: The Ocean Carbon Cycle, Annual Review of Environment and Resources, 47, 317–341, https://doi.org/10.1146/annurev-environ-120920-111307, 2022.
- Ermentrout, B.: Simulating, Analyzing, and Animating Dynamical Systems, Software, Environments, and Tools, Society for Industrial and Applied Mathematics, https://doi.org/10.1137/1.9780898718195, 2002.

- Friedlingstein, P., Cox, P., Betts, R., Bopp, L., von Bloh, W., Brovkin, V., Cadule, P., Doney, S., Eby, M., Fung, I., Bala, G., John, J., Jones, C., Joos, F., Kato, T., Kawamiya, M., Knorr, W., Lindsay, K., Matthews, H. D., Raddatz, T., Rayner, P., Reick, C., Roeckner, E., Schnitzler, K.-G., Schnur, R., Strassmann, K., Weaver, A. J., Yoshikawa, C., and Zeng, N.: Climate–Carbon Cycle Feedback Analysis: Results from the C4MIP Model Intercomparison, Journal of Climate, 19, 3337–3353, https://doi.org/10.1175/JCLI3800.1, 2006.
- Friedlingstein, P., Meinshausen, M., Arora, V. K., Jones, C. D., Anav, A., Liddicoat, S. K., and Knutti, R.: Uncertainties in CMIP5 Climate Projections due to Carbon Cycle Feedbacks, Journal of Climate, 27, 511–526, https://doi.org/10.1175/JCLI-D-12-00579.1, 2014.
- Friedlingstein, P., O'Sullivan, M., Jones, M. W., Andrew, R. M., Gregor, L., Hauck, J., Le Quéré, C., Luijkx, I. T., Olsen, A., Peters, G. P., Peters, W., Pongratz, J., Schwingshackl, C., Sitch, S., Canadell, J. G., Ciais, P., Jackson, R. B., Alin, S. R., Alkama, R., Arneth, A., Arora, V. K., Bates, N. R., Becker, M., Bellouin, N., Bittig, H. C., Bopp, L., Chevallier, F., Chini, L. P., Cronin, M., Evans, W., Falk, S., Feely, R. A., Gasser, T., Gehlen, M., Gkritzalis, T., Gloege, L., Grassi, G., Gruber, N., Gürses, Ö., Harris, I., Hefner, M., Houghton, R. A., Hurtt, G. C., Iida, Y., Ilyina, T., Jain, A. K., Jersild, A., Kadono, K., Kato, E., Kennedy, D., Klein Goldewijk, K., Knauer, J., Korsbakken, J. I., Landschützer, P., Lefèvre, N., Lindsay, K., Liu, J., Liu, Z., Marland, G., Mayot, N., McGrath, M. J., Metzl, N., Monacci, N. M., Munro, D. R., Nakaoka, S.-I., Niwa, Y., O'Brien, K., Ono, T., Palmer, P. I., Pan, N., Pierrot, D., Pocock, K., Poulter, B., Resplandy, L., Robertson, E., Rödenbeck, C., Rodriguez, C., Rosan, T. M., Schwinger, J., Séférian, R., Shutler, J. D., Skjelvan, I., Steinhoff, T., Sun, Q., Sutton, A. J., Sweeney, C., Takao, S., Tanhua, T., Tans, P. P., Tian, X., Tian, H., Tilbrook, B., Tsujino, H., Tubiello, F., van der Werf, G. R., Walker, A. P., Wanninkhof, R., Whitehead, C., Willstrand Wranne, A., Wright, R., Yuan, W., Yue, C., Yue, X., Zaehle, S., Zeng, J., and Zheng, B.: Global Carbon Budget 2022, Earth Syst. Sci. Data, 14, 4811-4900, https://doi.org/10.5194/essd-14-4811-2022, 2022.
- Geoffroy, O., Saint-Martin, D., Olivié, D. J. L., Voldoire, A., Bellon, G., and Tytéca, S.: Transient Climate Response in a Two-Layer Energy-Balance Model. Part I: Analytical Solution and Parameter Calibration Using CMIP5 AOGCM Experiments, Journal of Climate, 26, 1841–1857, https://doi.org/10.1175/JCLI-D-12-00195.1, 2013.
- Glotter, M. J., Pierrehumbert, R. T., Elliott, J. W., Matteson, N. J., and Moyer, E. J.: A simple carbon cycle representation for economic and policy analyses, Climatic Change, 126, 319–335, https://doi.org/10.1007/s10584-014-1224-y, 2014.
- Graham, R. J. and Pierrehumbert, R. T.: Carbon Cycle Instability for High-CO₂ Exoplanets: Implications for Habitability, Astrophysical Journal, 970, 32, https://doi.org/10.3847/1538-4357/ad45fb, 2024.
- Huntingford, C. and Mercado, L. M.: High chance that current atmospheric greenhouse concentrations commit to warmings greater than 1.5 °C over land, Scientific Reports, 6, 30294, https://doi.org/10.1038/srep30294, 2016.
- Huntingford, C., Cox, P. M., and Lenton, T. M.: Contrasting responses of a simple terrestrial ecosystem model

- to global change, Ecological Modelling, 134, 41–58, https://doi.org/10.1016/S0304-3800(00)00330-6, 2000.
- Huntingford, C., Booth, B. B. B., Sitch, S., Gedney, N., Lowe, J. A., Liddicoat, S. K., Mercado, L. M., Best, M. J., Weedon, G. P., Fisher, R. A., Lomas, M. R., Good, P., Zelazowski, P., Everitt, A. C., Spessa, A. C., and Jones, C. D.: IMOGEN: an intermediate complexity model to evaluate terrestrial impacts of a changing climate, Geosci. Model Dev., 3, 679–687, https://doi.org/10.5194/gmd-3-679-2010, 2010.
- Hülse, D. and Ridgwell, A.: Instability in the geological regulation of Earth's climate, Science, 389, eadh7730, https://doi.org/10.1126/science.adh7730, 2025.
- Jenkinson, D. S., Adams, D. E., and Wild, A.: Model estimates of CO₂ emissions from soil in response to global warming, Nature, 351, 1991.
- Jones, C. D. and Cox, P.: Constraints on the temperature sensitivity of global soil respiration from the observed interannual variability in atmospheric CO₂, Atmospheric Science Letters, 2, 166–172, https://doi.org/10.1006/asle.2001.0041, 2001.
- Jones, C. D., Hughes, J. K., Bellouin, N., Hardiman, S. C., Jones, G. S., Knight, J., Liddicoat, S., O'Connor, F. M., Andres, R. J., Bell, C., Boo, K.-O., Bozzo, A., Butchart, N., Cadule, P., Corbin, K. D., Doutriaux-Boucher, M., Friedlingstein, P., Gornall, J., Gray, L., Halloran, P. R., Hurtt, G., Ingram, W. J., Lamarque, J.-F., Law, R. M., Meinshausen, M., Osprey, S., Palin, E. J., Parsons Chini, L., Raddatz, T., Sanderson, M. G., Sellar, A. A., Schurer, A., Valdes, P., Wood, N., Woodward, S., Yoshioka, M., and Zerroukat, M.: The HadGEM2-ES implementation of CMIP5 centennial simulations, Geosci. Model Dev., 4, 543–570, https://doi.org/10.5194/gmd-4-543-2011, 2011.
- Joos, F., Bruno, M., Fink, R., Siegenthaler, U., Stocker, T. F., Le Quéré, C., and Sarmiento, J. L.: An efficient and accurate representation of complex oceanic and biospheric models of anthropogenic carbon uptake, Tellus B-Chemical and Physical Meteorology, 48, 397, https://doi.org/10.3402/tellusb.v48i3.15921, 1996
- Judd, E. J., Tierney, J. E., Lunt, D. J., Montañez, I. P., Huber, B. T., Wing, S. L., and Valdes, P. J.: A 485-million-year history of Earth's surface temperature, Science, 385, https://doi.org/10.1126/science.adk3705, 2024.
- Kageyama, M., Albani, S., Braconnot, P., Harrison, S. P., Hopcroft, P. O., Ivanovic, R. F., Lambert, F., Marti, O., Peltier, W. R., Peterschmitt, J.-Y., Roche, D. M., Tarasov, L., Zhang, X., Brady, E. C., Haywood, A. M., LeGrande, A. N., Lunt, D. J., Mahowald, N. M., Mikolajewicz, U., Nisancioglu, K. H., Otto-Bliesner, B. L., Renssen, H., Tomas, R. A., Zhang, Q., Abe-Ouchi, A., Bartlein, P. J., Cao, J., Li, Q., Lohmann, G., Ohgaito, R., Shi, X., Volodin, E., Yoshida, K., Zhang, X., and Zheng, W.: The PMIP4 contribution to CMIP6 Part 4: Scientific objectives and experimental design of the PMIP4-CMIP6 Last Glacial Maximum experiments and PMIP4 sensitivity experiments, Geosci. Model Dev., 10, 4035–4055, https://doi.org/10.5194/gmd-10-4035-2017, 2017.
- Marcott, S. A., Bauska, T. K., Buizert, C., Steig, E. J., Rosen, J. L.,
 Cuffey, K. M., Fudge, T. J., Severinghaus, J. P., Ahn, J., Kalk,
 M. L., McConnell, J. R., Sowers, T., Taylor, K. C., White, J.
 W. C., and Brook, E. J.: Centennial-scale changes in the global carbon cycle during the last deglaciation, Nature, 514, 616–619,
 https://doi.org/10.1038/nature13799, 2014.

- Munhoven, G.: Mathematics of the total alkalinity–pH equation pathway to robust and universal solution algorithms: the SolveSAPHE package v1.0.1, Geosci. Model Dev., 6, 1367–1388, https://doi.org/10.5194/gmd-6-1367-2013, 2013.
- Myhre, G., Highwood, E. J., Shine, K. P., and Stordal, F.: New estimates of radiative forcing due to well mixed greenhouse gases, Geophysical Research Letters, 25, 2715–2718, https://doi.org/10.1029/98GL01908, 1998.
- Petit, J. R., Jouzel, J., Raynaud, D., Barkov, N. I., Barnola, J.-M., Basile, I., Bender, M., Chappellaz, J., Davis, M., Delaygue, G., Delmotte, M., Kotlyakov, V. M., Legrand, M., Lipenkov, V. Y., Lorius, C., PÉpin, L., Ritz, C., Saltzman, E., and Stievenard, M.: Climate and atmospheric history of the past 420,000 years from the Vostok ice core, Antarctica, Nature, 399, 429–436, https://doi.org/10.1038/20859, 1999.
- Rothman, D. H.: Characteristic disruptions of an excitable carbon cycle, Proceedings of the National Academy of Sciences, 116, 14831–14822, https://doi.org/10.1073/pnas.1905164116, 2019.
- Saltzman, B. and Maasch, K. A.: Carbon cycle instability as a cause of the Late Pleistocene Ice Age Oscillations: Modeling the asymmetric response, Global Biogeochemical Cycles, 2, 177–185, https://doi.org/10.1029/GB002i002p00177, 1988.
- Sanderson, B. M., Booth, B. B. B., Dunne, J., Eyring, V., Fisher,
 R. A., Friedlingstein, P., Gidden, M. J., Hajima, T., Jones, C.
 D., Jones, C. G., King, A., Koven, C. D., Lawrence, D. M.,
 Lowe, J., Mengis, N., Peters, G. P., Rogelj, J., Smith, C., Snyder, A. C., Simpson, I. R., Swann, A. L. S., Tebaldi, C., Ilyina,
 T., Schleussner, C.-F., Séférian, R., Samset, B. H., van Vuuren,
 D., and Zaehle, S.: The need for carbon-emissions-driven climate projections in CMIP7, Geosci. Model Dev., 17, 8141–8172,
 https://doi.org/10.5194/gmd-17-8141-2024, 2024.
- Schimel, D., Stephens, B. B., and Fisher, J. B.: Effect of increasing CO₂ on the terrestrial carbon cycle, Proceedings of the National Academy of Sciences, 112, 436–441, https://doi.org/10.1073/pnas.1407302112, 2015.

- Sherwood, S. C., Webb, M. J., Annan, J. D., Armour, K. C., Forster, P. M., Hargreaves, J. C., Hegerl, G., Klein, S. A., Marvel, K. D., Rohling, E. J., Watanabe, M., Andrews, T., Braconnot, P., Bretherton, C. S., Foster, G. L., Hausfather, Z., von der Heydt, A. S., Knutti, R., Mauritsen, T., Norris, J. R., Proistosescu, C., Rugenstein, M., Schmidt, G. A., Tokarska, K. B., and Zelinka, M. D.: An Assessment of Earth's Climate Sensitivity Using Multiple Lines of Evidence, Reviews of Geophysics, 58, https://doi.org/10.1029/2019RG000678, 2020.
- Varney, R. M., Chadburn, S. E., Burke, E. J., Jones, S., Wiltshire, A. J., and Cox, P. M.: Simulated responses of soil carbon to climate change in CMIP6 Earth system models: the role of false priming, Biogeosciences, 20, 3767–3790, https://doi.org/10.5194/bg-20-3767-2023, 2023.
- Williamson, M. S., Cox, P. M., Huntingford, C., and Nijsse, F. J. M. M.: Testing the assumptions in emergent constraints: why does the "emergent constraint on equilibrium climate sensitivity from global temperature variability" work for CMIP5 and not CMIP6?, Earth Syst. Dynam., 15, 829–852, https://doi.org/10.5194/esd-15-829-2024, 2024.
- Zachos, J., Pagani, M., Sloan, L., Thomas, E., and Billups, K.: Trends, Rhythms, and Aberrations in Global Climate 65 Ma to Present, Science, 292, 686–693, https://doi.org/10.1126/science.1059412, 2001.
- Zelinka, M. D., Myers, T. A., McCoy, D. T., Po-Chedley, S., Caldwell, P. M., Ceppi, P., Klein, S. A., and Taylor, K. E.: Causes of Higher Climate Sensitivity in CMIP6 Models, Geophysical Research Letters, 47, 1–12, https://doi.org/10.1029/2019GL085782, 2020.